Sensitive Mach–Zehnder interferometric sensor based on a grapefruit microstructured fiber by lateral offset splicing

YU WANG,[1,2,5] YAN ZHOU,[1,5] ZHENGYONG LIU,[3,4] DARU CHEN,[1,*] CHAO LU,[2] AND HWA-YAW TAM[3]

[1]*Hangzhou Institute of advanced studies, Zhejiang Normal University, Hangzhou 311231, China*
[2]*Photonics Research Centre, Department of Electronic and Information Engineering, Hong Kong Polytechnic University, Hung Hom, Kowloon, Hong Kong*
[3]*Photonics Research Centre, Department of Electrical Engineering, Hong Kong Polytechnic University, Hung Hom, Kowloon, Hong Kong*
[4]*State Key Laboratory of Optoelectronic Materials and Technologies, School of Electronics and Information Technology, Sun Yat-sen University, Guangzhou 510275, China*
[5]*These authors contributed equally to this work*
*daru@zjnu.cn

Abstract: A novel inline Mach-Zehnder interferometric (MZI) sensor based on a homemade grapefruit microstructured fiber (GMF) was proposed and experimentally demonstrated. The sensing unit consists of a short segment of a GMF sandwiched between two single mode fibers using lateral offset splicing. The fabrication of the GMF and the GMF-based MZI sensor was introduced. Mode analysis of the GMF and theoretical simulation of the proposed MZI sensor were investigated and matched well with experimental results. The sensing performance of the MZI sensor for temperature and strain was tested. The strain and temperature sensitivity are 1.97$pm/\mu\varepsilon$ and 37$pm/$°C, respectively. The compact size, low cost and high sensitivity makes the MZI sensor a good candidate for sensing application.

1. Introduction

In the field of the optical fiber sensors, Fiber Bragg gratings (FBGs) [1,2,3] and long period fiber gratings (LPGs) [4,5,6] which are fabricated in the conventional single mode fiber (SMF) by employing expensive equipment such as a femtosecond laser or a UV excimer laser with high intensity, are the most well-known fiber sensors for such as temperature or strain sensing. However, various types of optical fiber sensors which are fabricated by splicing a segment of special optical fibers [7,8,9] to the SMF simply using a low-cost fiber fusion splicer have also been developed in recent years [10]. Microstructured optical fibers (MOFs) have attracted considerable attention over the past several decades due to their potential application in fiber sensor [11,12,13], fiber communication [14,15] and fiber laser [16]. Numbers of fiber sensors based on MOFs have been widely used for physical parameter sensing, such as temperature, strain, torsion, pressure and humidity owing to their well-known advantages like flexible design, compact size, light weight, immunity to electromagnetic interference, and high stability in harsh environment.

Most MOFs and photonic crystal fibers (PCFs) based sensors were realized based on the multimode interference, especially the interference between the fundamental mode and the first high-order mode [17]. However, the visibility of fringe pattern is very low since the transmission intensity of the fundamental mode is much higher than the higher order mode, which greatly limits the performance of the fiber sensors in practical applications. In order to enhance intensity of the higher order mode, the suspended core fiber with small core and large air holes have been introduced, which means more complicated fiber fabrication and splicing technics are essential and the fiber will be more fragile [18,19]. Another works [20,21] reported the use of

fiber tapers to construct a Mach-Zehnder interferometer (MZI). However, the relative refractive index difference of the core mode and the cladding mode is small, resulting the long distance between the two tapers which is necessary to provide sufficient light path difference for sensing application, and the taper would be vulnerable and sensitive to surrounding environment.

In this paper, a novel MZI sensor based on the grapefruit microstructured fiber (GMF) is proposed to achieve temperature and strain sensing. The GMF was designed and fabricated in our laboratory and the MZI sensor was fabricated by splicing a short segment of a GMF between two SMFs, where only a commercial fusion splicer was used to realize lateral offset alignment. The first offset point was used to split light into both the fiber core and the air hole of the GMF, and the second one combined the interference light into the lead-out SMF. By optimizing the air hole arrangement and size in fiber cross-section of the GMF, the proposed MZI sensor is insensitive to surrounding refractive index (SRI) and humidity. The fringe pattern with high quality can be achieved by adjusting the lateral offset to control different energy distribution in the fiber core and the air hole. The theoretical analysis and experimental setup of the fiber design and the sensor fabrication have been demonstrated, and the temperature and strain sensing performance of the MZI sensor has been investigated.

2. Fiber fabrication and working principle

2.1. Fiber fabrication and simulation

The GMF was fabricated in Photonics Research Center, Hong Kong Polytechnic University, using stack-and-draw technique as shown in Fig. 1(a). The parameters of the silica tube and capillaries are listed in the Table 1.
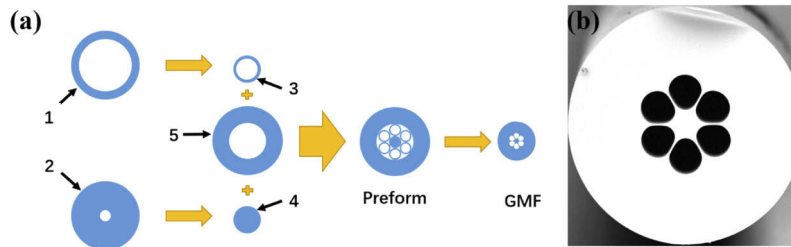
Fig. 1. Fabrication process of the GMF. (a) Schematic of fabrication process using stack-and-draw technique (b) SEM image of the GMF cross-section

Table 1. The parameters of the silica tubes and capillaries used in the fabrication process.

	Inner diameter	Outer diameter
Tube 1	25 mm	19 mm
Tube 2	22.5 mm	4 mm
Capillary 3	1.33 mm	1 mm
Rod 4	1.33 mm	0 mm
Tube 5	12 mm	4 mm

Firstly, capillary 3 and rod 4 were drawn from glass tube 1 and glass tube 2, respectively. Then, stack the preform of GMF in tube 5, where the rod 4 is placed in the center, surrounded by six capillaries 3. Finally, draw the preform into designed fiber with an outer diameter of 125μm. The cross-section scanning electron microscopic (SEM) photo of the drawn fiber is shown in

Fig. 1(b), the suspended fiber core with a diameter about 14μm was surrounded by six air holes with diameters about 20μm.

Simulation was carried out through the full-vector finite element method (FEM). Figure 2(a) shows the effective refractive index of the x-polarized and y-polarized fundamental modes of the GMF in the wavelength range from 1570 nm to 1590 nm by scanning wavelengths with a step of 1 nm. It can be observed that the effective index difference is small and each can be chosen to analyze the MZI transmission spectrum. Mode field distribution of x-polarized and y-polarized fundamental modes of the GMF at wavelength of 1580 nm were shown in Figs. 2(b) and 2(c), respectively.
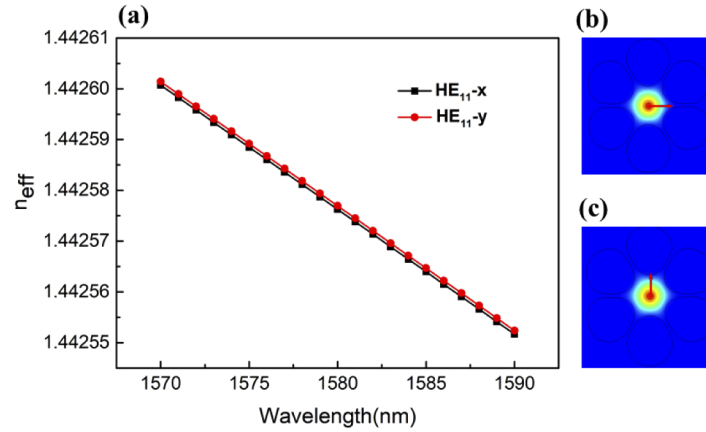
Fig. 2. (a) Effective refractive index of the x-polarized (black curves) and y-polarized (red curves) fundamental modes of the GMF. (b) and (c) show the mode profile of the power flow of the x- and y-polarized fundamental mode at the wavelength of 1580 nm respectively.

2.2. Working principle

The schematic diagram of the proposed MZI sensor is shown in Fig. 3(a). The light launched from a broadband source (BBS) will transmit along the fiber core of the lead-in SMF, and be split into the air hole (air mode) and the fiber core of the GMF (core mode) in the offset splicing point due to the mode field mismatch. Note that the air mode is a leaked mode with the transmission property similar as that in free space. The part of the injected light coupled into the air hole will recouple into the fiber core of the lead-out SMF in the second splicing point and interfere with the light transmitted through the fiber core of the GMF, and the visibility of interference pattern was controlled by adjusting the lateral offset displacement.

The transmission intensity of the MZI could be expressed as:

$$I(\lambda) = I_{core}(\lambda) + I_{air}(\lambda) + 2\sqrt{I_{core}I_{air}}\cos(\phi) \tag{1}$$

where I_{core}, I_{air} are the transmission intensities of the light transmitted through the suspended core and the air holes of the GMF, respectively, and ϕ is the phase difference between them. The optical path and the intensity of the two modes are not the same due to the effective refractive index difference between the two modes and loss caused by splicing, which result in accumulated phase difference that can be described as:

$$\phi = 2\pi L(n_{core} - n_{air})/\lambda_0 \tag{2}$$

here L is the length of GMF and λ_0 is the operating wavelength in vacuum. n_{core} and n_{air} is effective refractive index of the two modes that propagate in the suspended core and the air holes
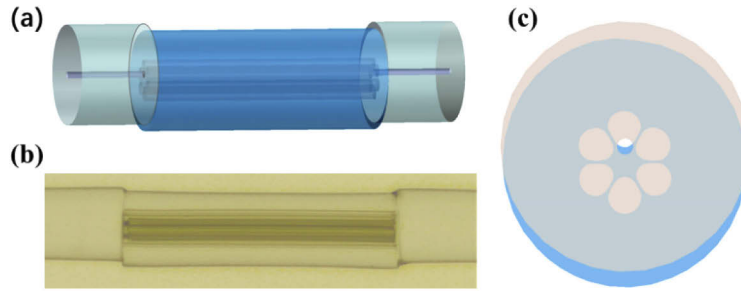
Fig. 3. (a) Schematic illustration of proposed structure. (b) microscopy image of the proposed sensing unit. (c) schematic diagram of the cross-section image in splicing joint

of GMF, respectively. The transmission dip can be achieved when phase difference satisfies the condition $\phi = (2m + 1)\pi$, and the dip wavelength can express as:

$$\lambda_m = \frac{2(n_{core} - n_{air})L}{2m + 1} \tag{3}$$

where m is an integer. The wavelength spacing between two adjacent interference dip is

$$\Delta\lambda_{dip} = \frac{4(n_{core} - n_{air})L}{(2m - 1)(2m + 1)} \approx \frac{\lambda^2}{(n_{core} - n_{air})L} \tag{4}$$

According to simulation result in Fig. 3, the transmission spectrum of our MZI structure can be calculated and is shown in Fig. 4 with the length of the GMF set as 500μm, 1000μm, 1500μm, 2000μm, respectively. In our calculation, the intensity of the double modes was set as the same. The spectrum is a sinusoidal curve and the wavelength spacing can be calculated.
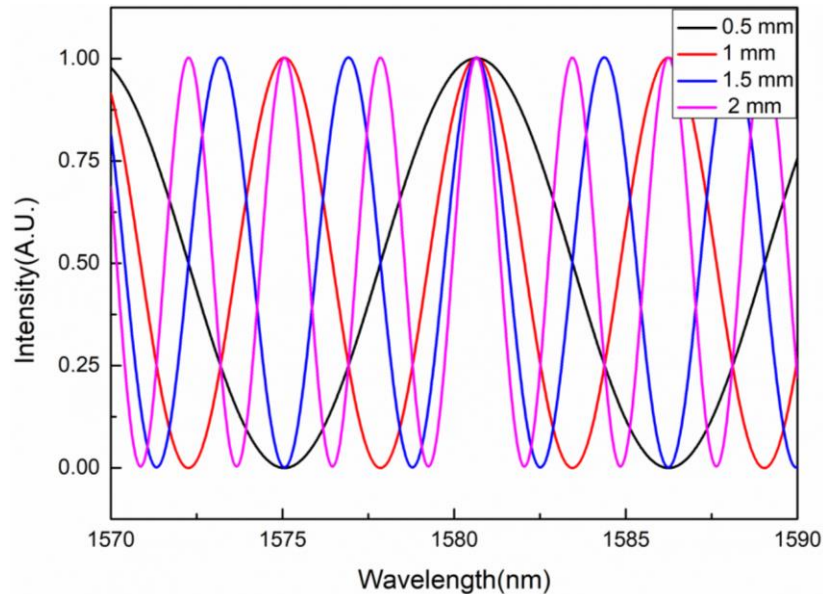
Fig. 4. Simulated interference spectra of the MZI structure based on GMFs with a length of 0.5 mm, 1 mm, 1.5 mm and 2 mm, respectively.

3. Experiment setup and result

3.1. MZI fabrication

The fabrication process of the MZI structure is shown in Fig. 5(a). The incident light emitted from a BBS was launched into the lead-in SMF and transmitted through the GMF, then the transmission spectrum was collected by an optical spectrum analyzer (OSA). Firstly, one SMF was spliced with a segment of the GMF by a fusion splicer (Fujikura 80S), with lateral offset of several microns, which was optimized by gradually enlarge the offset displacement from 0 to 8 microns with different GMF length. Next, pigtail of a GMF was cut down and the length was adjusted with the help of a microscope and a homemade precision cutting platform. After that, the right end of the GMF was spliced to the lead-out SMF to form the MZI structure. Since the visibility of interference fringes was determined by the relative intensity of $I_{core}(\lambda)$ and $I_{air}(\lambda)$. The offset position of the second joint should be carefully adjusted in the fusion splicer to ensure the lateral offset of the SMFs in the same direction. That means the light transmitted through the air holes have best coupling efficiency into the lead-out SMF. The lateral offset displacement was another important parameter to achieve a high-performance sensor. Too small displacement between the lead-in SMF and the GMF means most of the energy was restricted in the core of the GMF, and it is hard to achieve high spectrum visibility by only adjusting the second splicing point. However, large displacement between the lead-in SMF and the GMF results in the large insertion loss and also the low spectrum visibility.
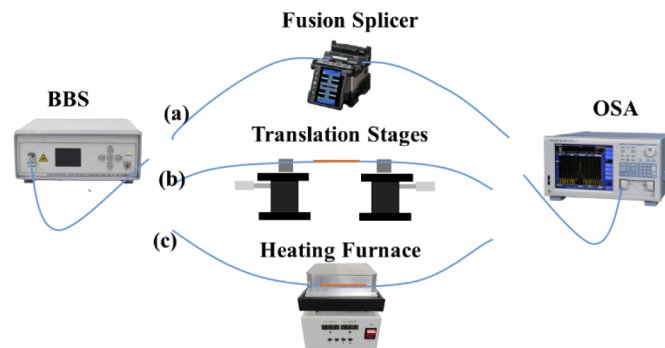

Fig. 5. Schematic diagram of the setup for MZI fabrication and sensing performance test.

Figure 6(a) shows two typical transmission spectra with different offset directions and same offset value about 5μm, which was optimized by multi-attempts according to our specific experimental equipment and arc parameters. The red and black lines correspond to results before and after optimizing relative position, respectively. It is easy to draw a conclusion that carefully adjusting the second splicing position plays a vital role in fabricating our MZI structure. In order to minimize the distortion of the GMF, the discharge power and duration time was set as -60 bit and 400 ms by multiple attempts and optimizing. According to Eq. (4), the wavelength spacing between two adjacent interference dip varies inversely as the length of GMF. In our experiment, different lengths of GMFs have been fabricated and the transmission spectrum is illustrated in Fig. 6(b). The fast Fourier transform (FFT) of transmission spectra illustrated above is adopted to demonstrate the validity of theoretical analysis. The dominate interference peaks appear at frequency of $0.0859nm^{-1}$, $0.1772nm^{-1}$, $0.2627nm^{-1}$ and $0.3667nm^{-1}$, corresponding to the GMF length of 500μm, 1000μm, 1500μm and 2000μm, respectively. The relationship between $\Delta\lambda_{dip}$ and length L in our experiment also have been analyzed and the result matched well with the theoretical value which is calculated as the interference between the air mode and

the core fundamental mode that we demonstrated in Fig. 2. That results are shown in Figs. 6(c) and 6(d), respectively.
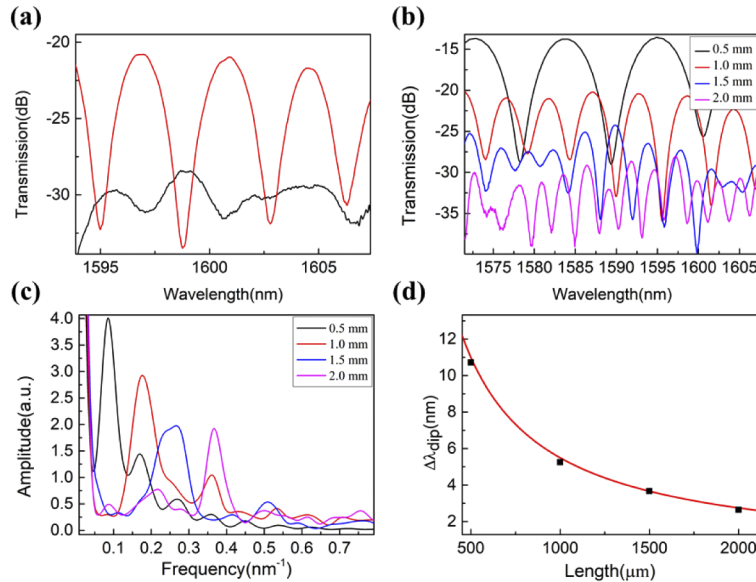

Fig. 6. (a) transmission spectra with different lateral offset splicing direction (b)transmission spectrum with a 0.5 mm, 1 mm, 1.5 mm,2 mm long GMF, respectively. (c)FFT of spectrum showed in (b). (d) Theoretical calculation curve (red curve) and experimental result (black dots) of the relationship between $\Delta\lambda_{dip}$ and length L at 1590 nm.

3.2. Strain response

The experiment setup for strain response testing is demonstrated in Fig. 5(b). A segment of a GMF with length of 500μm was offset spliced with two SMF pigtails and fixed onto a pair of 3D translation stages by two fiber holders with v-groove among them, and the distance between them is 10 cm. The light launched from a BBS with a wavelength range from 1520 nm to 1620 nm, and the transmission light was collected by an OSA (Yokogawa 6375) with a resolution of 0.05 nm. The translation stages moved away 60μm with the same interval of 2μm. Transmission spectra were illustrated in Fig. 7(a). The applied strain on the MZI sensor results in the length increasement of the GMF together with the red shift of the interference spectra, which can be easily derived from Eq. (3). The wavelength dip around 1588 nm as a function of strain was given in Fig. 7(b). Linear fitting was conducted and the sensitivity for strain sensing is $1.97 pm/\mu\varepsilon$ and the R-square is 0.9985. According to the definition of normalized strain, the cavity length of proposed MZI sensor will not affect the strain sensitivity but the dynamic range. The longer length of the MZI cavity will result in the smaller stress applied on the splicing point under the same strain.

3.3. Temperature response

Temperature response of the proposed MZI structure was carried out by fixing the sensor part in a homemade heating furnace, which increased the temperature from 30°C to 180°C with a step of 10 °C. The schematic setup was illustrated in Fig. 5(c). The evolution of transmission spectra in different temperature have been recorded and are shown in Fig. 8(a). The wavelength dip near 1600 nm is chosen for analyzing. With the rising of temperature, red shift of the dip happened
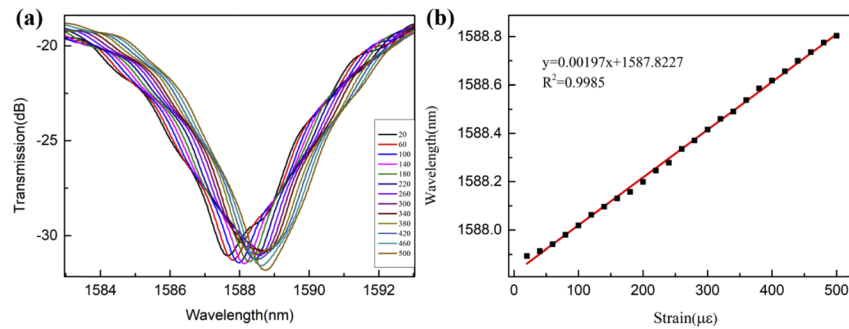
Fig. 7. (a) Spectral response of proposed MZI sensor with a 500μm long GMF for different Strain. (b)Dip wavelength versus different strain. The red curve is linear fitting result.

due to the thermo-expansion of the MZI structure. By linear fitting process, the sensitivity for temperature response is obtained as $37pm/°C$ and R-square is 0.9991. That is more sensitive than commercial FBG temperature sensors which have been widely used in industry. According to Eq. (3), the temperature sensitivity was related to the cavity length and the RI difference between the core mode and air mode. Since the large RI difference between the two modes, our proposed fiber sensor can provide a high sensitivity with small size such as 500μm, and that is an important indicator for point temperature sensing performance.
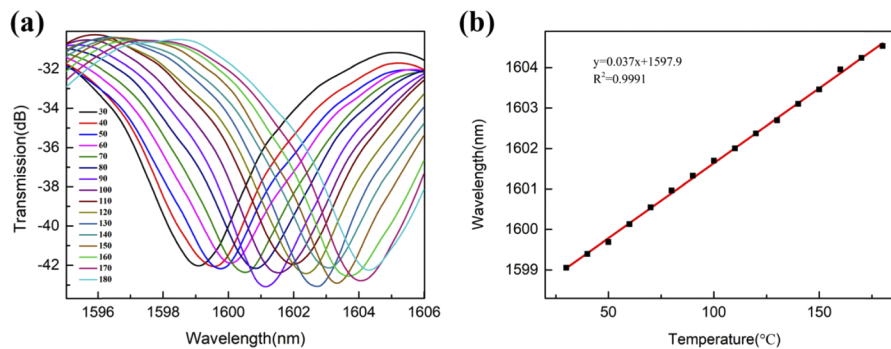
Fig. 8. (a) Spectral evolution of MZI sensors for temperature variation from 30°C to 180°C. (b) Dip wavelength versus different temperature. The red curve is linear fitting result.

4. Conclusion

We have designed and fabricated an inline MZI sensor for temperature and strain sensing. This proposed fiber sensor was formed by inserting a segment of a GMF between two SMFs with the help of only a simply optical fiber fusion splicer. The fabrication of the GMF and simulation of the mode field of the GMF have been illustrated. Theoretical analysis of interference phenomenon for the GMF based MZI structure has been demonstrated, which matched well with experimental results. Strain and temperature response of the MZI sensor have been carried out. Experimental results show that sensitivity for strain and temperature sensing is $1.97pm/\mu\varepsilon$ and $37pm/°C$, respectively. By cascading several proposed MZI sensors with precisely manipulated cavity lengths and utilizing Fast Fourier Transform (FFT) to complex transmission spectra of multi-point MZI sensors, we can demodulate the change in each cavity lengths by phase shift of different amplitude peak in FFT spectra [22], which realizes the multi-point sensing capability based on

the proposed MZI sensors. The proposed MZI sensor is simple-structured, high sensible and compact in size which make it a good candidate for future application.

Funding

Disclosures

The authors declare no conflicts of interest.

References

1. A. Othonos, "Fiber Bragg gratings," Rev. Sci. Instrum. **68**(12), 4309–4341 (1997).
2. Y. Yu, H. Tam, W. Chung, and M. Demokan, "Fiber Bragg grating sensor for simultaneous measurement of displacement and temperature," Opt. Lett. **25**(16), 1141–1143 (2000).
3. H. J. Patrick, G. M. Williams, A. D. Kersey, J. R. Pedrazzani, and A. M. Vengsarkar, "Hybrid fiber Bragg grating/long period fiber grating sensor for strain/temperature discrimination," IEEE Photonics Technol. Lett. **8**(9), 1223–1225 (1996).
4. C. Lin, L. Wang, and G. Chern, "Corrugated Long-Period Fiber Gratings as Strain, Torsion, and Bending Sensors," J. Lightwave Technol. **19**(8), 1159–1168 (2001).
5. Y. Rao, Y. Wang, Z. Ran, and T. Zhu, "Novel Fiber-Optic Sensors Based on Long-Period Fiber Gratings Written by High-Frequency CO2 Laser Pulses," J. Lightwave Technol. **21**(5), 1320–1327 (2003).
6. C. Ye, S. James, and R. Tatam, "Simultaneous temperature and bend sensing with long-period fiber gratings," Opt. Lett. **25**(14), 1007–1009 (2000).
7. Y. Wang, G. Yan, Z. Lian, C. Wu, and S. He, "Liquid-level sensing based on a hollow core Bragg fiber," Opt. Express **26**(17), 21656–21663 (2018).
8. L. Jin, B. Guan, and H. Wei, "Sensitivity Characteristics of Fabry-Perot Pressure Sensors Based on Hollow-Core Microstructured Fibers," J. Lightwave Technol. **31**(15), 2526–2532 (2013).
9. L. Xiao, W. Jin, M. S. Demokan, H. L. Ho, Y. L. Hoo, and C. L. Zhao, "Fabrication of selective injection microstructured optical fibers with a conventional fusion splicer," Opt. Express **13**(22), 9014–9022 (2005).
10. G. Salceda-Delgado, A. Van Newkirk, J. Antonio-Lopez, A. Martinez-Rios, A. Schülzgen, and R. Amezcua Correa, "Compact fiber-optic curvature sensor based on super-mode interference in a seven-core fiber," Opt. Lett. **40**(7), 1468–1471 (2015).
11. C. Wu, B. Guan, Z. Wang, and X. Feng, "Characterization of Pressure Response of Bragg Gratings in Grapefruit Microstructured Fibers," J. Lightwave Technol. **28**(9), 1392–1397 (2010).
12. Y. Lizé, E. Mägi, V. Ta'eed, J. Bolger, P. Steinvurzel, and B. Eggleton, "Microstructured optical fiber photonic wires with subwavelength core diameter," Opt. Express **12**(14), 3209–3217 (2004).
13. V. Minkovich, J. Villatoro, D. Monzón-Hernández, S. Calixto, A. Sotsky, and L. Sotskaya, "Holey fiber tapers with resonance transmission for high-resolution refractive index sensing," Opt. Express **13**(19), 7609–7614 (2005).
14. J. Tu, Z. Liu, S. Gao, Z. Wang, J. Zhang, B. Zhang, J. Li, W. Liu, H. Tam, Z. Li, C. Yu, and C. Lu, "Ring-core fiber with negative curvature structure supporting orbital angular momentum modes," Opt. Express **27**(15), 20358–20372 (2019).
15. J. Tu, B. Zhang, Z. Liu, X. Zhou, K. Long, Z. Li, C. Lu, and C. Yu, "Chalcogenide-Glass Nested Anti-Resonant Nodeless Fibers in Mid-Infrared Region," J. Lightwave Technol. **36**(22), 5244–5253 (2018).
16. X. Jiang, B. Mao, Y. Wei, D. Chen, L. She, G. Feng, and J. Yang, "Wavelength-tunable all-fiber mode-locked laser based on supermode interference in a seven-core fiber," Appl. Opt. **57**(23), 6768–6771 (2018).
17. Y. Zheng, P. Shum, Y. Luo, Y. Zhang, W. Ni, G. Wang, Z. Wu, X. Dinh, J. Auguste, and G. Humbert, "High-resolution, large-dynamic-range multimode interferometer sensor based on a suspended-core microstructured optical fiber," Opt. Lett. **45**(4), 1017–1020 (2020).
18. L. Htein, Z. Liu, D. Gunawardena, and H. Tam, "Single-ring suspended fiber for Bragg grating based hydrostatic pressure sensing," Opt. Express **27**(7), 9655–9664 (2019).
19. X. Zhang, X. Zhu, and Y. Shi, "Fiber optic surface plasmon resonance sensor based on a silver-coated large-core suspended-core fiber," Opt. Lett. **44**(18), 4550–4553 (2019).
20. Y. F. Geng, X. J. Li, X. L. Tan, Y. L. Deng, and Y. Q. Yu, "High-sensitivity Mach–Zehnder interferometric temperature fiber sensor based on a waist-enlarged fusion bitaper," IEEE Sens. J. **11**(11), 2891–2894 (2011).
21. P. Wang, G. Brambilla, M. Ding, Y. Semenova, Q. Wu, and G. Farrell, "High-sensitivity, evanescent field refractometric sensor based on a tapered, multimode fiber interference," Opt. Lett. **36**(12), 2233–2235 (2011).
22. C. Wang, G. Yan, Z. Lian, X. Chen, S. Wu, and S. He, "Hybrid-cavity Fabry-Perot interferometer for multi-point relative humidity and temperature sensing," Sens. Actuators, B **255**, 1937–1944 (2018).